STARS

2017

Combustion of 1,3-Butadiene behind Reflected Shocks

Joseph Lopez
University of Central Florida

Part of the Aerodynamics and Fluid Mechanics Commons

Find similar works at: https://stars.library.ucf.edu/etd

University of Central Florida Libraries http://library.ucf.edu

STARS Citation

University of Central Florida

STARS

Showcase of Text, Archives, Research & Scholarship

COMBUSTION OF 1,3-BUTADIENE
BEHIND REFLECTED SHOCKS

by

JOSEPH G. LOPEZ
B.S. University of Central Florida, 2015

A thesis submitted in partial fulfillment of the requirements
for the degree of Master of Science
in the Department of Mechanical and Aerospace Engineering
in the College of Engineering and Computer Science
at the University of Central Florida
Orlando, Florida

Spring Term
2017

Major Professor: Subith S. Vasu

ABSTRACT

The chemical kinetics of 1,3-butadiene (1,3-C_4H_6) are important because 1,3-butadiene is a major intermediate during the combustion of real fuels. However, there is only limited information on the chemical kinetics of 1,3-butadiene combustion, which has applications in several combustion schemes that are currently being developed, including spark-assisted homogeneous charge compression ignition and fuel reformate exhaust gas recirculation.

In the present work, the ignition delay times of 1,3-butadiene mixtures has been investigated using pressure data. Oxidation of 1,3-butadiene/oxygen mixtures diluted in argon or nitrogen at equivalence ratios (Φ) of 0.3 behind reflected shock waves has been studied at temperatures ranging from 1100 to 1300K and at pressures ranging from 1 to 2atm. Reaction progress was monitored by recording concentration time-histories of 1,3-butadiene and OH* radical at a location 2cm from the end wall of a 13.4m long shock tube with an inner diameter of 14cm. 1,3-Butadiene concentration time-histories were measured by absorption spectroscopy at 10.5μm from the P14 line of a tunable CO_2 gas laser. OH* production was measured by recording emission around 306.5nm with a pre-amplified gallium phosphide detector and a bandpass filter. Ignition delay times were also determined from the OH* concentration time-histories. The measured concentration time-histories and ignition delay times were compared with two chemical kinetics models. The measured time-histories and ignition delay times provide targets for the refinement of chemical kinetic models at the studied conditions.

I dedicate this to my grandparents, *Gardenio* and *Maria Mata*, whose love, support and influence made me the person I am today.

Dedico esto a mis abuelos, *Gardenio* y *Maria Mata*, cuyo amor, apoyo e influencia me hicieron la persona que soy hoy.

ACKNOWLEDGMENTS

Firstly, I would like to thank my fiancée *Noa Frank* for all her affection and encouragement throughout my academic endeavors. I would also like to thank my parents, *Gustavo* and *Diane Lopez* as well as my siblings, *Angel* and *Jennifer Font* for their support and optimism towards my enthusiasm for fire even from a young age.

I would like to thank my advisor *Dr. Subith Vasu* for all the guidance and knowledge he gave me over the past four years; as well as, my committee members *Dr. Nina Orlovskaya* and *Dr. Alain Kassab* for their roles associated with their positions.

I would like to thank all of my colleagues from the University of Central Florida; especially, *Bader Almansour* and *Dr. Batikan Koroglu* for teaching me the foundations of combustion during my first year of research and *Leigh Nash*, *Zach Loparo*, *Owen Pryor* and *Bob Wong* for their supportive efforts towards my research.

TABLE OF CONTENTS

LIST OF FIGURES

LIST OF TABLES

NOMENCLATURE

1,3-C_4H_6	1,3-Butadiene
α_λ	Absorbance
σ_i	Absorption Cross Section of Species i (cm^2/mol)
Ar	Argon
CO_2	Carbon Dioxide
OH*	Excited Hydroxyl Radicals
OH	Hydroxyl Radicals
R	Ideal Gas Constant (cm^2 atm / mol K)
LLNL	Lawrence Livermore National Laboratory
HgCdTe	Mercury Cadmium Telluride
CH	Methyl Radials
x_i	Mole Fraction of Species i
N_2	Nitrogen
L	Optical Path Length (cm)
O_2	Oxygen
PTFE	Polytetrafluoroethylene
P5	Pressure behind the Reflected Shock Wave
I_0	Reference Intensity
T	Temperature (K)
T5	Temperature behind the Reflected Shock Wave
P_{tot}	Total Pressure (atm)
I	Transmitted Intensity
ZnSe	Zinc Selenide

CHAPTER ONE: INTRODUCTION

1.1: 1,3-Butadiene

1,3-Butadiene (1,3-C_4H_6) is a small alkene having four carbon atoms. At room temperature and pressure 1,3-butadiene exists in a gaseous phase, attributed to its vapor pressure of 1800Torr at 20C [1]. During the combustion process of large hydrocarbons, like those typically found in gasoline, diesel and jet fuels, smaller hydrocarbons are formed as the atomic bonds of the larger hydrocarbon molecules break and rearrange. Therefore the combustion process of typical hydrocarbon fuels is highly dependent on the reaction pathway it takes to reach the final products, ideally carbon dioxide (CO_2), water and in most cases some diluent.

1,3-Butadiene is an integral intermediate species during the combustion of larger hydrocarbons and therefore it is imperative to study 1,3-butadiene combustion to increase the fidelity of modern hydrocarbon fuel combustion modeling [2-4]. Furthermore, 1,3-butadiene has been found in the exhaust emissions of automobiles and aircrafts as a product of incomplete combustion which is not only undesired because of the apparent decrease in efficiencies of any unburned hydrocarbons but also because 1,3-butadiene is known to be highly carcinogenic to humans and animals [5]. Although 1,3-butadiene released into the atmosphere undergoes several reactions mainly leading to the formation of acrolein and formaldehyde, atmospheric 1,3-butadiene can still be found in urban and suburban areas [5].

The chemical kinetics of 1,3-butadiene combustion has applications in several combustion schemes that are currently being developed, including spark-assisted homogeneous charge compression ignition and fuel reformate exhaust gas recirculation [6, 7].

1.2: Shock Tube Theory

The basis of shock tube theory is nested in the concept that gases at any pressure differentials which are allowed to interact on one another will attempt to equilibrate. At high pressure differentials, which value's depends on the ratio of specific heat capacities and the speed of sound of both the high and low pressure gases and assuming sufficient run-up distance is given, isentropic pressure waves will coalesce in the flow and form an adiabatic shock wave that travels through the system increasing the temperature and pressure of the gas and imparting a velocity in the direction the shock wave is traveling.

Typical shock tubes are separated into two major sections called the driver and driven sections, associated with the high and low pressure sides of the system, respectively. The driver section is typically filled with a gas with a relatively high ratio of specific heat capacities and relatively low atomic weight, which propagates into a high speed of sound gas and ultimately correlating to a stronger shock wave. The driven section is filled with the test mixture being studied. In a shock tube, the process of reaching equilibrium after the driver and driven gases are allowed to act on one another causes three main gas dynamics effects to occur within the system, the formation of: an incident shocks wave though the test mixture in the driven section, a contact surface between the gases in the driver and driven propagating in the direction of the driven section as would be suggested by the pressure differential and expansion waves in the direction of the driver.

Although the incident shock wave and contact surface both travel in the same direction the incident shock wave travels much faster and therefore reaches the end wall of the driven section sooner. Upon interaction between the incident shock wave and the end wall, a reflected shock wave is formed and travels in the opposite direction as the incident shock wave does as the

2

test mixture is brought to a quiescent state. The kinetic energy associated with the test mixture's velocity imparted by the passage of the incident shock is converted into an increase of temperature and pressure, this process is illustrated in Figure 1 and is sometimes referred to as, "shock heating" [8, 9].

The time before the reflected shock wave and contact surface interact at any certain longitudinal location is referred to as the test time of the experiment at that circumferential plane and is a measure of the maximum time interval that can be studied at the constant elevated temperature and pressure behind the reflected shock.
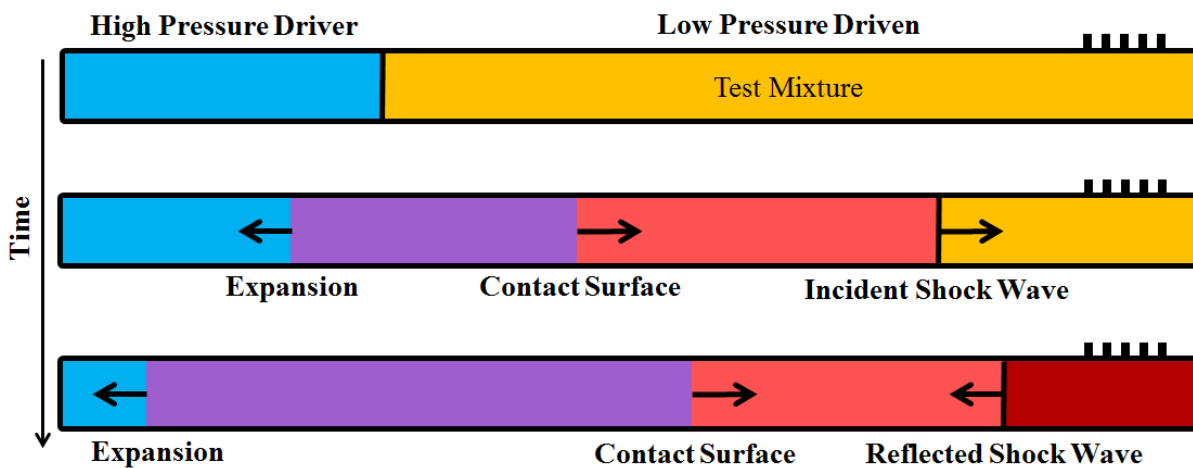
Figure 1: Shock tube concept

A more detailed graphical approach to understanding the phenomena within the shock tube is the x-t diagram, which plots the propagation of the major gas dynamics effects as a function of longitudinal location and time; an x-t diagram of a generic shock is shown in Figure 2.
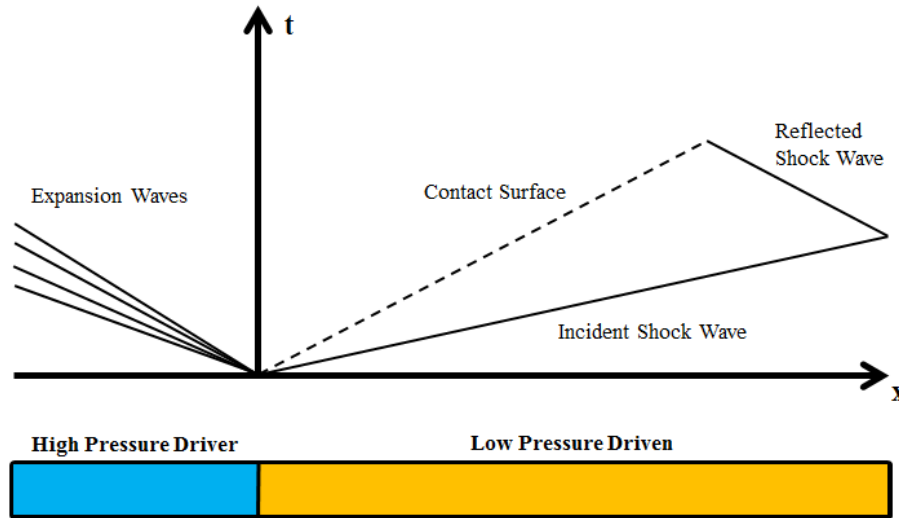
Figure 2: x-t Diagram of a generic shock

1.3: Optical Diagnostics

Optical diagnostic are among the best measurement techniques for any fluid flow-based system due to the highly non-intrusive nature of low power radiation on flowing systems, unlike direct measurement techniques [10]. Three types of optical diagnostic techniques are employed in this study: ultraviolet emissions and direct laser absorption, the theory of each is discussed in the respective subsection.

1.3.1: Ultraviolet Emissions

Due to the quantized nature of electron energy transitions of an atom or molecule, assertions about a certain excited species can be made by focusing on a particular wavelength associated with the energy between electron transition levels [11, 12]. Therefore, by filtering spectral emissions of a highly energetic system, like combustion, one is able to target the presence of an excited species as it releases photons associated with an energy level transition. In

this work, the ultraviolet emissions of excited hydroxyl radicals (OH*) are measured and used to assess trends associated with the presence of radical species during the ignition of 1,3-butadiene.

1.3.2: Direct Laser Absorption

Direct laser absorption is a widely used technique for accurately determining path line averaged target species concentrations through the use of absorption spectroscopy [13, 14]. The theoretical basis for absorption spectroscopy is the relation between the attenuation of light traveling through a medium and the medium itself, defined by the Beer-Lambert Law shown in Equation 1 [14].

$$\alpha_\lambda = -\ln\left(\frac{I}{I_o}\right)_\lambda = \sigma_i(\lambda,\ T, P)\frac{P_{tot}}{RT} x_i\ L \qquad (1)$$

Where α_λ is the absorbance at a particular wavelength, I is the transmitted intensity, I_0 is the reference intensity, σ_i is the absorption cross section of species i (cm^2/mol), P_{tot} is the total pressure (atm), T is the temperature (K), R is the ideal gas constant (cm^2 atm / mol K), x_i is the mole fraction of species i and L is the optical path length (cm).

1.4: Combustion and Chemical Kinetics

The combustion process of hydrocarbon fuels and oxidizers is more complex than the one step chemical reactions typically used to convey simple chemistry concepts. In reality, the combustion of hydrocarbon fuels is dependent on the chemical breakdown to simpler species, in many cases atomic species, which react to produce stable products. Radicals, a class of highly reactive and unstable species, are created in a process known as initiation where a stable species breakdowns to form at least one radical. Following initiation, radicals react via: propagation,

branching or termination corresponding to the net result of radicals produced by the reaction being either zero, positive or negative, respectively.

Chemical kinetics is the foundation of understanding combustion from a chemical reaction perspective. Two important chemical kinetics parameters are measured in this work, ignition delay times and species time-histories.

One important parameter of a combustible mixture is the fuel-oxidizer equivalence ratio (Φ), this quantity is defined as the ratio between the actual molar fuel-oxidizer ratio of the mixture and the stoichiometric fuel-oxidizer ratio, shown in Equation 2.

$$\Phi = \frac{\left(N_{fuel}\Big/N_{oxidizer}\right)_{Actual}}{\left(N_{fuel}\Big/N_{oxidizer}\right)_{stoichiometric}} \tag{2}$$

Where N represents the number of moles for the subscripted component. The fuel-oxidizer equivalence ratio is used to quantitatively determine if a combustible mixture is fuel lean, stoichiometric or fuel lean.

1.4.1: Ignition Delay Times

The ignition delay time of a certain combustible mixture can be defined as the time interval at a particular temperature and pressure before the onset of ignition; the trouble lies in the definition of the term, "ignition" [14-16]. Ignition can be defined as the point of maximum radical concentration, maximum rate of radical formation extrapolated to a baseline value of radicals (typically zero), the point when 2/3 of the initial fuel concentration is depleted or by the maximum rate of pressure increase extrapolated to a baseline value of pressure; graphical

6

representations of each of these definitions is shown in Figure 3, since only the trends of excited

hydroxyl radical emissions are considered the emissions are normalized to their peak value.
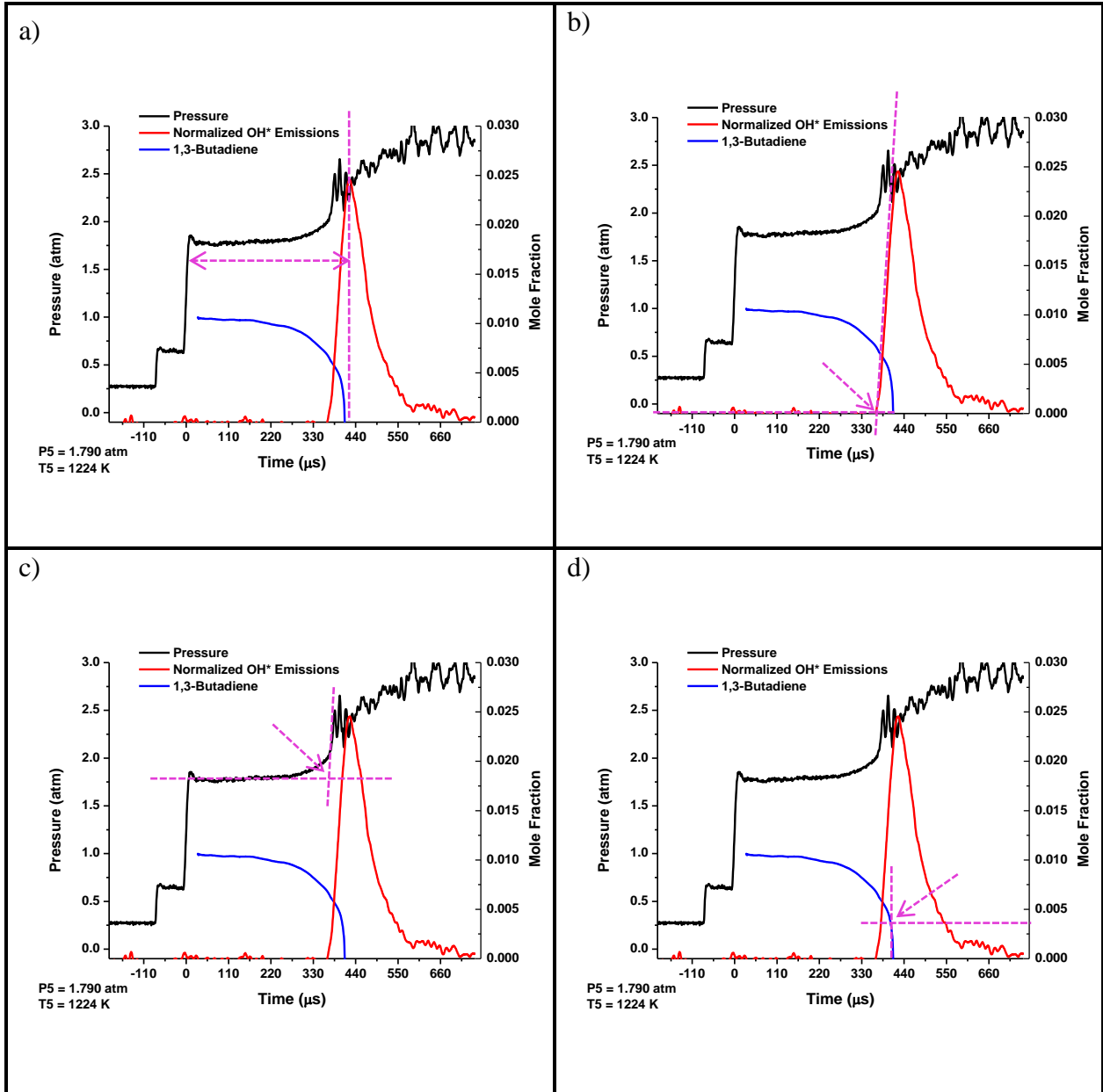
Figure 3: Ignition delay time definitions – a) maximum radical concentration, b) maximum rate of radical formation extrapolated to a baseline value of radicals, c) maximum rate of pressure increase extrapolated to a baseline value of pressure, d) 2/3 of the initial fuel concentration.

Practically, the ignition delay time of a fuel at a particular temperature and pressure is a critical parameter of engine performance and optimization and therefore is highly studied [14-19]. Due to the practicality constraints of measuring all radical species during combustion, it is very common to focus on one radical species; the most common are hydroxyl (OH) and methyl (CH) radicals.

1.4.2: Species Time-Histories

The concentration of a particular species as a function of time during a chemical reaction is referred to as the time-history of that species. The species time-history is dictated by the concentration of all species present and the reaction rate constants of all possible reactions taking place at the conditions present. Therefore, reaction rate information can be obtained by measuring species time-history during a chemical reaction. In this work, such a method is employed by determining the species time-history of 1,3-butadiene.

CHAPTER TWO: LITERATURE REVIEW

2.1: 1,3-Butadiene Combustion

Although 1,3-butadiene combustion has been studied for over 30 years, very limited literature exists on lean 1,3-butadiene combustion; alternatively, rich 1,3-butadiene combustion has been studied to a great extent [2-4, 20-22].

2.1.1: Flat Flame Burners

Rich 1,3-butadiene combustion has been studied using flat flame burners by Cole et al. and Hansen et al, see Table 1, these studies focused on species concentrations as a function of distance from the burner measured by mass spectrometry techniques [2, 20]. Table 1 shows a literature summary of experimental condition for 1,3-butadiene combustion studied in flat flame burners.

Table 1: Flat flame burner - literature summary

Apparatus	Phi	1,3-C_4H_6 (%)	Diluent Species	Pressure (atm)	Temperature (K)	References
Flat Flame Burner	2.4	29.5	Ar	0.026	-	Cole et al. [20]
Flat Flame Burner	1.8	7.6	Ar	0.039	-	Hansen et al. [2]

2.1.2: Reactors

1,3-Butadiene combustion has also been studied in flow and jet stirred reactors over a wide range of conditions by Brezinsky et al., Dagaut et al. and Laskin et al. [3, 4, 22]. The chemical kinetics of 1,3-butadiene combustion was studied through species concentrations measured by flame ionization detectors, thermal conductivity detectors and mass spectrometry techniques [3, 4, 22]. Table 2 shows a literature summary of experimental condition for 1,3-butadiene combustion studied in reactors.

Table 2: Reactors - literature summary

Apparatus	Phi	1,3-C_4H_6 (%)	Diluent Species	Pressure (atm)	Temperature (K)	References
Flow Reactor	1.18	0.143	N_2	1	1125	Brezinsky et al. [22]
Flow Reactor	1.65	0.143	N_2	1	1125	Brezinsky et al. [22]
Jet Stirred Reactor	0.25	0.15	N_2	1	750 - 1250	Dagaut et al. [3]
Jet Stirred Reactor	0.5	0.15	N_2	10	750 - 1250	Dagaut et al. [3]
Jet Stirred Reactor	1	0.15	N_2	1	750 - 1250	Dagaut et al. [3]
Jet Stirred Reactor	1	0.15	N_2	10	750 - 1250	Dagaut et al. [3]
Flow Reactor	0.55	0.14	N_2	1	1035 - 1120	Laskin et al. [4]
Flow Reactor	1	0.14	N_2	1	1120	Laskin et al. [4]
Flow Reactor	1.62	0.144	N_2	1	1110	Laskin et al. [4]
Flow Reactor	1.63	0.142	N_2	1	1035	Laskin et al. [4]
Flow Reactor	4.7	0.14	N_2	1	1120	Laskin et al. [4]

Prior to this work, 1,3-butadiene combustion was only studied in a shock tube by Fournet et al.; who focused on moderate pressures from 8.5-10atm [21]. The ignition delay times of 1,3-butadiene mixtures were measured by excited hydroxyl radical emissions measured with a photomultiplier tube and monochromator assembly.

To the best of the author's knowledge, the present work is the first one which measures 1,3-butadiene time-histories during combustion in a shock tube at high temperatures by direct absorption spectroscopy. Table 3 shows a literature summary of experimental condition for 1,3-butadiene combustion studied in shock tubes.

Table 3: Shock tube - literature summary

Apparatus	Phi	1,3-C_4H_6 (%)	Diluent Species	Pressure (atm)	Temperature (K)	References
Shock Tube	0.69	1	Ar	8.5 - 10	1300 - 1500	Fournet et al. [21]
Shock Tube	1.38	1	Ar	8.5 - 10	1300 - 1700	Fournet et al. [21]
Shock Tube	1.38	3	Ar	8.5 - 10	1200 - 1500	Fournet et al. [21]
Shock Tube	0.3	1	Ar	1.0 - 2.0	1150 - 1250	This Work
Shock Tube	0.3	1.13	N_2	1	1200 - 1300	This Work
Shock Tube	0.5	1	Ar	1.4 - 1.6	1100 - 1300	This Work

CHAPTER THREE: EXPERIMENTAL SETUP

3.1: Manifold and Mixing Tank

The foundation of all experiments conducted for this work is the reactive gas mixtures which are studied at target conditions behind a reflected shock. The mixtures studied in this work were created manometrically using a ten-port manifold and mixing tank assembly.

The mixing tank utilized in this study was constructed from 304-stainless steel, the internal volume of the mixing tank is 33L and the entire internal volume is Polytetrafluoroethylene (PTFE) coated for both chemical compatibility between the steel surface of the mixing tank and the reactive gases and also to maintain low surface roughness by filling any small pores or cavities of the steel surface that condensed liquids may adhere to. The physique of the mixing tank is separated into three sections the: upper blind flange, central cylindrical body, and lower blind flange. A fluoroelastomer O-ring is used to make the seal between the blind flange sections and the cylindrical body. A heating jacket for the mixing tank can be utilized to increase the mixing tank's wall temperature when using reagents of low vapor pressures at room temperature but this heating system was not required for the range of experiments included in this work.

The ten port manifold (Figure 4) utilized for this work was used to couple the mixing tank, shock tube and reagent cylinders. The manifold was equipped with two capacitance manometers (MKS Baratron E27D and 628D, accuracies of 0.12% and 0.25% of reading, respectively) used to accurately measure the pressure within the mixing tank and shock tube during the mixture creation process and mixture introduction, respectively. An isolation valve was placed inline of the 100Torr range capacitance manometer and was used to manually ensure

the manometer was never exposed to pressures above the specified tolerance of the unit. The entire body of the manifold is constructed of 316-stainless steel. All ports on the manifold are fitted with bellow seal valves (Swagelok SS-4H-VCR) utilized to maintain a low leak rate across the valves despite high pressure differentials.
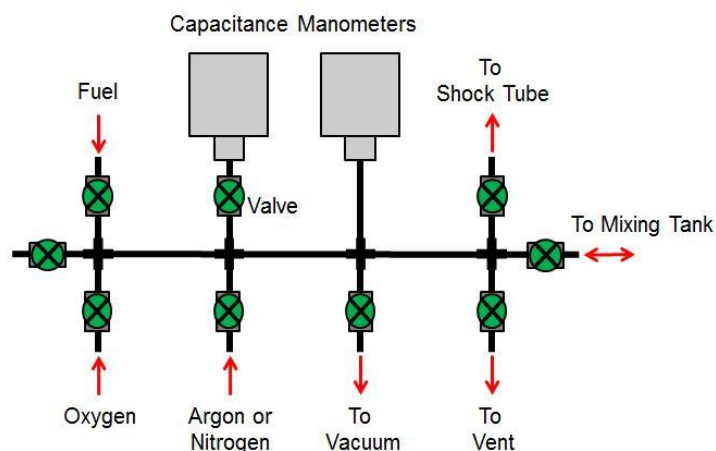
Figure 4: Manifold schematic

Prior to creating a mixture, the mixing tank was evacuated below 5.00×10^{-5} Torr, measured by an ion gauge (Lesker KJLC354401YF), using a turbo molecular pump (Agilent model V301). This was done to ensure a high fidelity mixture was created by minimizing the error associated with the presence of extraneous species in the mixture.

Mixtures were prepared manometrically at room temperature by partial pressure contribution to the total mixture pressure. Prior to the introduction of a new mixture component, the supply line was pressurized and evacuated three or more times to create a flow which purges the supply lines and manifold with that component. After the manifold was purged with a new component and directly prior to introducing the new component into the mixing tank, the manifold was pressurized higher than the mixing tank to mitigate the effects of back flow from

13

the tank into the manifold which would cause for an erroneous mixture from the loss of some unmixed mixture.

Prior to mixture introduction into the shock tube, the mixture was left in the mixing tank for about six hours to homogenize though diffusion.

3.1.1: Chemicals and Reagents

Throughout the facilities used for this work, many chemicals and reagents are used. All gas species used in this work are of high purity, nitrogen (99.999%), oxygen(99.999%), argon(99.999%) and helium(99.999%) were purchased from Nexair,; 1,3-butadiene (>99%) was purchased from (Sigma-Aldrich 295035).

3.2: The Shock Tube

The stainless steel shock tube (inner diameter of 14.17cm) with driver and driven sections separated by a polycarbonate diaphragm of thickness about 127μm, other thicknesses are possible and available but were not used in this study. The inner surface of the driven section is electro-polished to reduce the effects of surface nucleated reactions and boundary layer effects.

Prior to the experiment, both sections of the shock tube are evacuated by rotary vein pumps (Agilent DS102). After the pressure in the driven section is sufficiently low (< 200mTorr), measured by convection gauge (Lesker KJL275804LL), to engage a turbo molecular pump (Agilent model V301), the driven section is isolated from the rotary vein pumps and the turbo molecular pump and driven section are integrated. The driven section is left to further evacuate to below 5.00×10^{-5}Torr, measured by an ion gauge (Lesker KJLC354401YF); after which, the driver and driven sections are isolated from all vacuuming systems.

To initiate the shock process, and thus the experiment, the test mixture previously created in the mixing tank was introduced into the shock tube though the manifold. The pressure and temperature of the test mixture filled driven section are measured utilizing the capacitance manometers coupled to the manifold and a T-type thermocouple imbedded in-line between the manifold and driven section. The driven section and manifold are then isolated from one another and the driver section is filled with pure helium gas. After a short time, the pressure differential across the driver and driven sections causes the diaphragm to rapidly deflect towards the driven section where it makes contact with an in-house fabricated cutter. Eventually, the interaction between the diaphragm and cutter causes a sudden rupture of the diaphragm which, in turn, creates the large pressure differential to initiate the shock heating process. All pressure and spectroscopic data presented in this work are taken at a location 2cm away from the end wall of the driven side of the shock tube.

3.2.1: Shock Velocity

Due to the viscous effects of the test mixture the incident shock wave does not travel at a constant velocity. Therefore it is necessary to determine the attenuation of the incident shock's velocity as a function of distance traveled. In this work, the incident shock attenuation was measured by use of five piezoelectric pressure transducers (PCB 113B26) coupled to four time-interval counters (Agilent 53220A). The distance between each piezoelectric pressure transducer was measured and in conjunction with the time value measured with the time-interval counters an accurate determination of the shock velocity is achieved. By means of linear regression an extrapolated value for the velocity, and thus Mach number, of the incident shock at the end wall of the driven section is determined. This extrapolated Mach number is used to predict the

strength of the reflected shock wave and provides the basis for the conditions behind the reflected shock wave.

3.2.2: Pressure

The pressure at a location 2cm away from the driven section end wall is measured using a piezoelectric pressure transducer (Kistler 603B1), this pressure trace is used to determine the arrival of the reflected shock wave and the available test time. In this work only combustible mixtures are studied and therefore all pressure data recorded shows an increase in pressure at the time of ignition due to energy release associated with the combustion process. A schematic of the pressure measurement system can be seen in Figure 5.

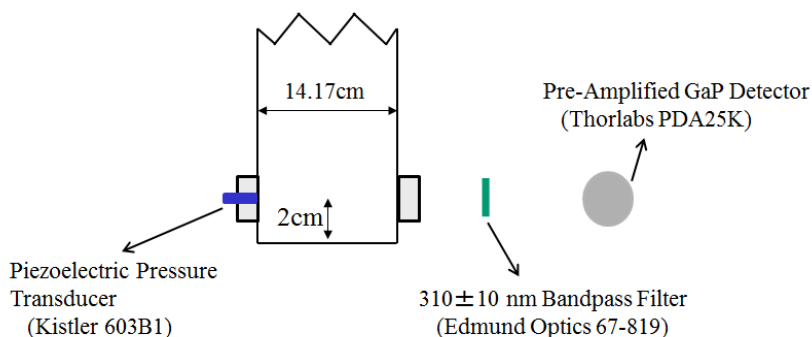**Figure 5: Pressure and emission measurement schematic**

3.3: Spectroscopic Measurements

This study employs three different types of optical measurements: ultraviolet emissions from excited hydroxyl radicals (OH*), direct absorption spectroscopy of 1,3-butadiene and atomic resonance absorption spectroscopy of hydrogen atoms, each of which is discussed in further detail in the following sections.

3.3.1: Ultraviolet Emissions

The ultraviolet emissions of OH* was measured with a pre-amplified gallium phosphide (GaP) detector (Thorlabs PDA25K) with detection range of 150 - 550nm, a 310±10 nm bandpass Filter (Edmund Optics 67-819) was integrated with the GaP detector in order to focus on the emissions of OH* at 306.5nm [11]. A schematic of the ultraviolet emissions detection system is can be seen in above in Figure 5 with the pressure measurement system.

3.3.2: Direct Absorption Spectroscopy

Direct absorption spectroscopy of 1,3-butadiene was achieved in this study by means of a continuous waveform CO_2 laser (Access Laser L4GS) operated at the P14 transition near 10.532 μm. In order to decrease the intensity of the laser power a neutral density filter (Thorlabs NDIR10A) was placed directly in front of the laser's transmission port, similar to the works done by Stranic et al. [23]. After the neutral density filter, a beam splitter was used to create two beam paths: one for transmission through the shock tube and one for referencing any fluctuations in the laser's output, further on referred to as the transmission beam and reference beam, respectively. The reference beam was directed through an iris and made incident on a photovoltaic mercury cadmium telluride (HgCdTe) detector (Vigo PVI-3TE-10.6, Optimal Wavelength of 10.6μm). The transmission beam was directed though an iris, then a set of zinc selenide (ZnSe) windows (Thorlabs WW70530) of the shock tube, followed by a 10.00±2.0μm bandpass filter (Andover Corp. 10.00GA40-25) to reduce the effects of extraneous radiation produced by black body emission of gases in the shock tube during the combustion process, the beam is then reflected on to another photovoltaic mercury cadmium telluride (HgCdTe) detector (Vigo PVI-3TE-10.6) by a curved mirror used to maintain the alignment of the beam on the detector's surface despite

slight beam steering effects caused by the refractive index change associated with the sharp density gradients across the shock waves, a phenomena sometimes referred to as "Schlieren spike" [24, 25]. A schematic of the direct absorption spectroscopy system can be seen in Figure 6.
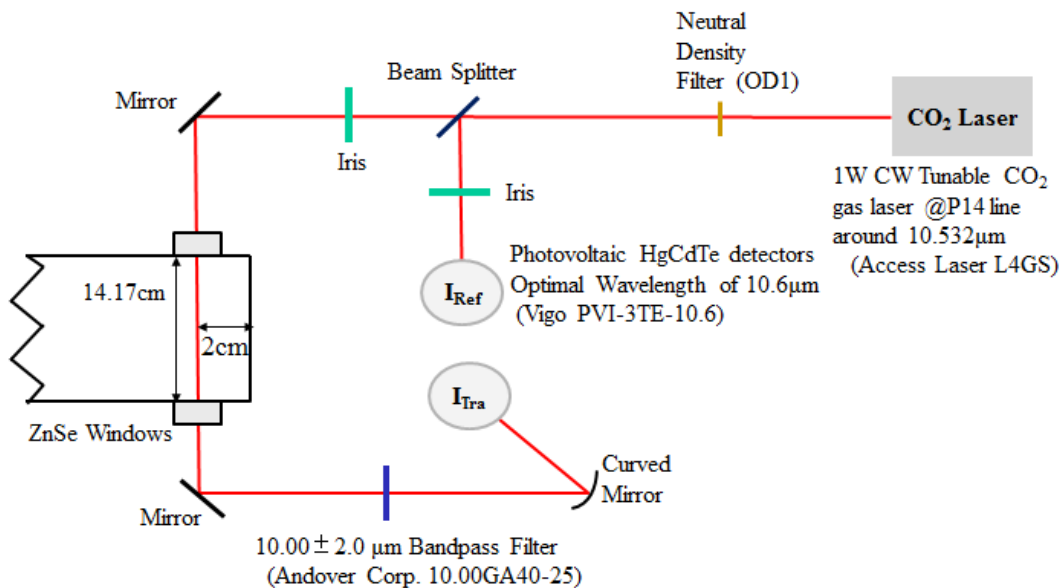

Figure 6: Direct absorption spectroscopy system for 1,3-butadiene

CHAPTER FOUR: RESULTS AND DISCUSSION

In this work, the ignition delay times and 1,3-butadiene species time histories are reported for lean mixtures of 1,3-butadiene and oxygen (O_2) diluted in argon (Ar) and nitrogen (N_2) at pressures ranging from about 1atm to 2atm and temperatures ranging from about 1100K to 1300K. Results are compared against two common chemical kinetics mechanism, Aramco 2.0 mechanism and Lawrence Livermore National Laboratory (LLNL) Gasoline Surrogate mechanism using CHEMKIN PRO to test each mechanism's predictability [26, 27].

Three 1,3-butadiene/oxygen mixtures sets were studied in this work, $\Phi = 0.3$-argon diluted, $\Phi = 0.5$-argon diluted and $\Phi = 0.3$-nitrogen diluted. Table 4 shows the relevant mixture information and experimental conditions studied of each mixture, the uncertainty of the temperature and pressure is estimated to be less than ±1%.

Table 4: Mixture information and experimental conditions

Mixture Information				
Φ	Percent 1,3-Butadiene	Diluent Species	Temperature (K)	Pressure (atm)
0.3	1%	Ar	1143	1.927
0.3	1%	Ar	1224	1.790
0.3	1%	Ar	1142	1.031
0.3	1%	Ar	1171	1.651
0.3	1%	Ar	1232	1.451
0.5	1%	Ar	1289	1.439
0.5	1%	Ar	1091	1.614
0.5	1%	Ar	1124	1.427
0.3	1.13%	N_2	1296	1.035
0.3	1.13%	N_2	1241	1.091
0.3	1.13%	N_2	1192	1.134

4.1: Ignition Delay Times

The ignition delay time of each mixture and condition was determined by each of the four ignition delay time definition discussed above. Table 5, Table 6 and Table 7 show the ignition delay time results of the $\Phi = 0.3$-argon diluted mixture and the average value is reported for comparison.

Table 5: Ignition delay time for the $\Phi = 0.3$-argon diluted mixture

Temperature (K)	Pressure (atm)	Ignition Delay Time (µs)				
		Emissions Peak	Emissions Baseline	Pressure Baseline	2/3rd Fuel Depletion	Average
1143	1.927	1422.5	1364.1	1375.3	1381.0	1385.7
1224	1.790	424.5	372.2	373.4	391.5	390.4
1142	1.031	2104.0	2071.3	2101.6	2047.5	2081.1
1171	1.651	1012.5	987.2	990.1	988.0	994.5
1232	1.451	495.5	447.8	439.3	451.0	458.4

Table 6: Ignition delay time for the $\Phi = 0.5$-argon diluted mixture

Temperature (K)	Pressure (atm)	Ignition Delay Time (µs)				
		Emissions Peak	Emissions Baseline	Pressure Baseline	2/3rd Fuel Depletion	Average
1289	1.439	360.0	337.7	335.1	334.0	341.7
1091	1.614	4081.0	4038.2	4017.2	4058.5	4048.7
1124	1.427	2888.5	2830.2	2844.1	2851.5	2853.6

20

Table 7: Ignition delay time for the Φ = 0.3-nitrogen diluted mixture

Temperature (K)	Pressure (atm)	Ignition Delay Time (μs)				
		Emissions Peak	Emissions Baseline	Pressure Baseline	2/3rd Fuel Depletion	Average
1296	1.035	177.5	126.4	131.5	145.0	145.1
1241	1.091	449.5	376.2	368.0	405.5	399.8
1192	1.134	1232.7	1045.2	1015.3	1412.0	1176.3

The spread of the ignition delay times shown above is well within the ±18% estimated uncertainty of the measurement. It can be seen that the ignition delay time is a function of temperature and pressure, where increasing either will decrease the ignition delay time.

4.2: Species Time-Histories

1,3-Butadiene time-history measurements, taken by absorption spectroscopy using a CO_2 laser, for each mixture and experimental condition are provided below in Figure 7, Figure 8 and Figure 9. Since the absorption cross section for 1,3-butadiene was not determined in this work, the 1,3-butadiene mole fraction of the mixture was used to determine the initial mole fraction from the spectroscopic measurement. T5 and P5 represent the temperature and pressure of the test mixture behind the reflected shock wave, respectively.
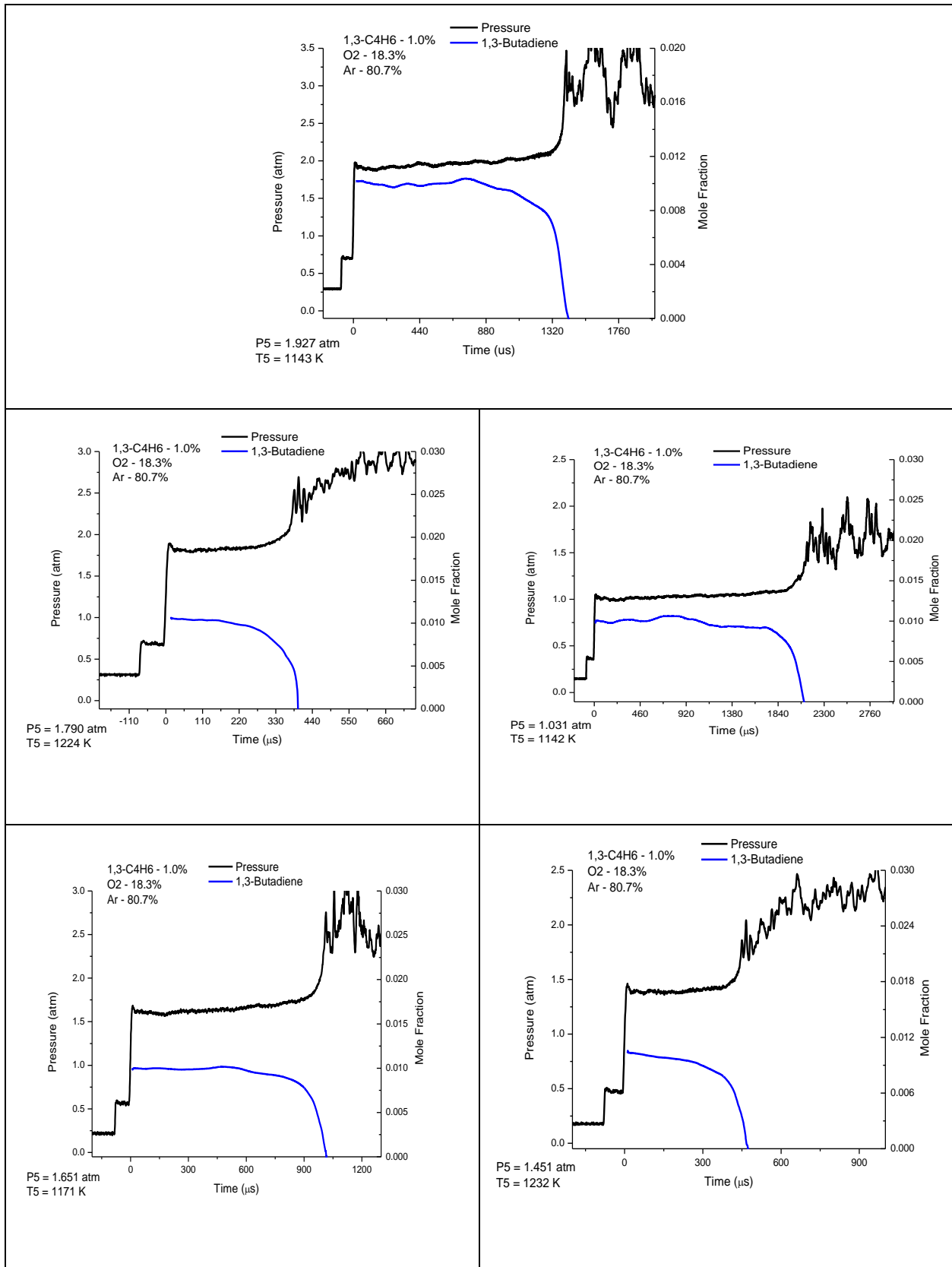
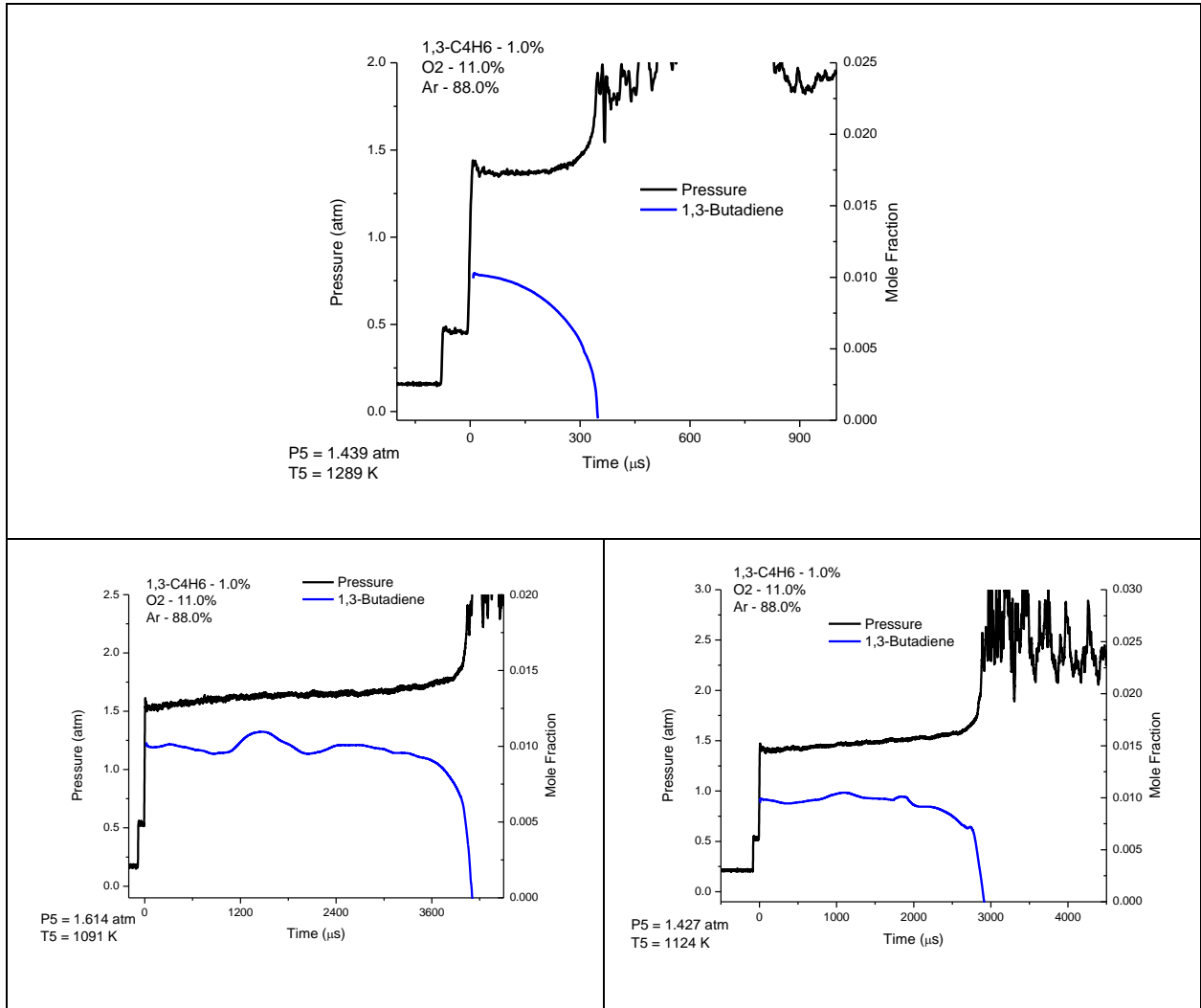**Figure 7: 1,3-Butadiene time histories for the Φ = 0.3-argon diluted mixture**

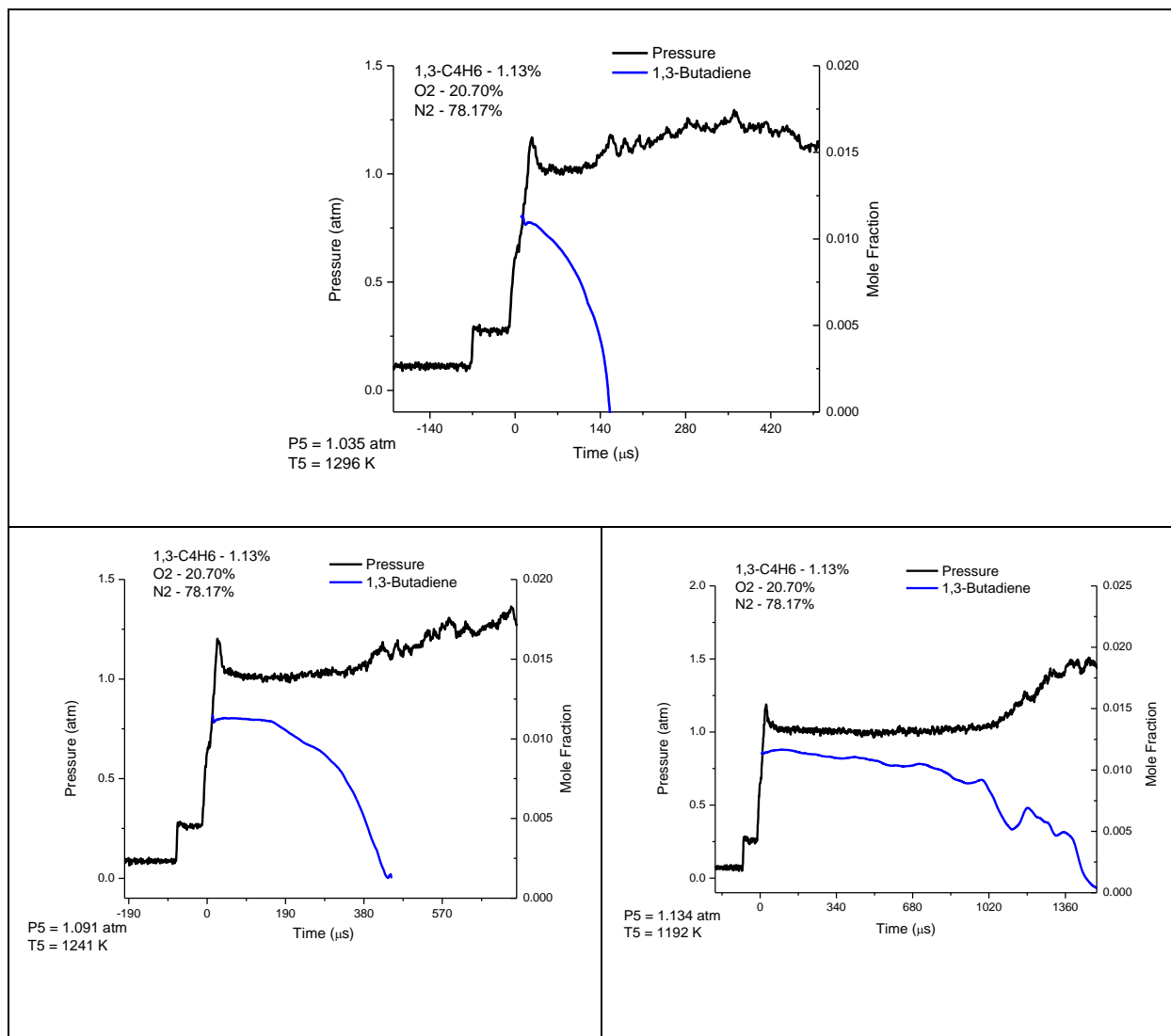**Figure 8: 1,3-Butadiene time histories for the Φ = 0.5-argon diluted mixture**

Figure 9: 1,3-Butadiene time histories for the Φ = 0.3-nitrogen diluted mixture

4.3: Comparison with Simulations

The ignition delay times and 1,3-butadiene time-histories were compared with two common chemical kinetics mechanisms, Aramco 2.0 mechanism and Lawrence Livermore National Laboratory (LLNL) Gasoline Surrogate mechanism, CHEMKIN PRO was utilized to evaluate the mechanisms at the experimental conditions. As can be seen in Figure 10, the pressure behind the reflected shock wave in all presented data is approximately constant; for this

reason, the chemical kinetics modeling for both the ignition delay times and 1,3-butadiene time-histories was done under constant pressure and internal energy assumptions.
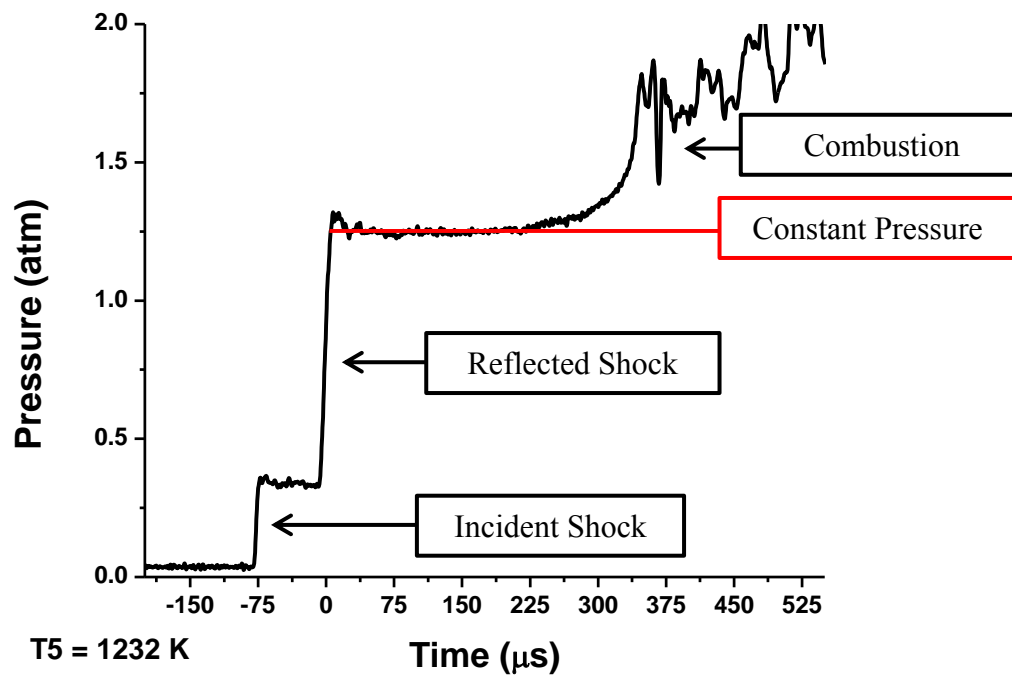

Figure 10: Sample pressure traces with constant pressure behind reflected shock

Experimental results and simulations do not agree for the combustion of lean 1,3-butadiene mixtures to a significant extent which can be seen in Figure 11 .
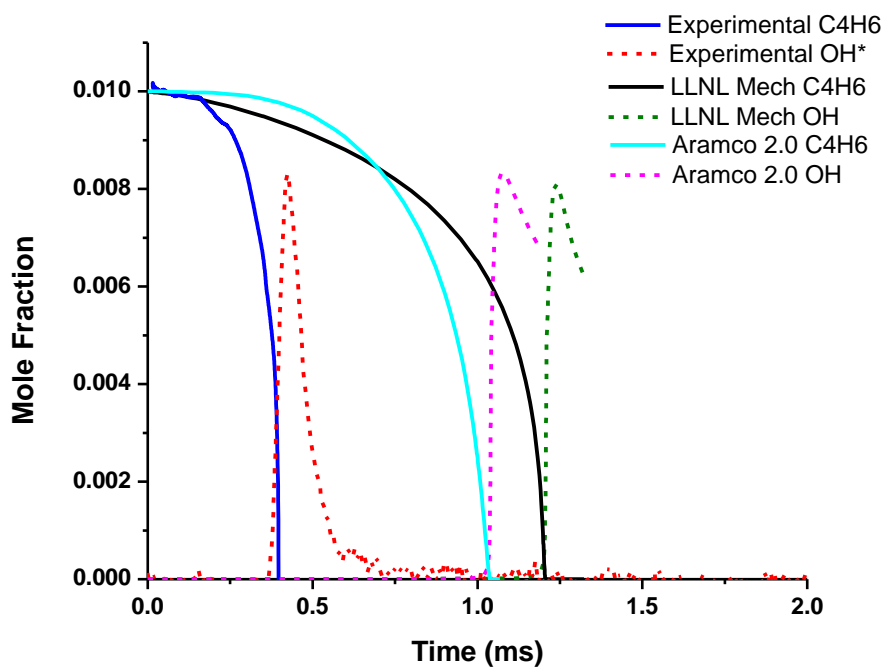
Figure 11: Sample comparison between experimental data and simulations

4.3.1: Ignition Delay Time Modeling

For comparative purposes, only the peak concentration of excited hydroxyl radicals will be used to determine the ignition delay time for each chemical kinetics mechanism. Table 8, Table 9 and Table 10 show a comparison between the experimental and simulated ignition delay times.

Table 8: Ignition delay time comparison for the Φ = 0.3-argon diluted mixture

Temperature (K)	Pressure (atm)	Ignition Delay Time (µs)		
		Emissions Peak	LLNL	Aramco 2.0
1143	1.927	1423	7455	8212
1224	1.790	424.5	1631	1355
1142	1.031	2104	10071	10000
1171	1.651	1013	4515	4294
1232	1.451	495.5	1570	1287

Table 9: Ignition delay time comparison for the Φ = 0.5-argon diluted mixture

Temperature (K)	Pressure (atm)	Ignition Delay Time (µs)		
		Emissions Peak	LLNL	Aramco 2.0
1289	1.439	360	902	690
1091	1.614	4081	36647	43545
1124	1.427	2889	18686	17641

Table 10: Ignition delay time comparison for the Φ = 0.3-nitrogen diluted mixture

Temperature (K)	Pressure (atm)	Ignition Delay Time (µs)		
		Emissions Peak	LLNL	Aramco 2.0
1296	1.035	177.5	760	666
1241	1.091	449.5	1647	1377
1192	1.134	1233	3763	3326

It can be seen that both chemical kinetics mechanisms are not in agreement with the experimental values of ignition delay times in any mixture. This is most likely due to the lack of experimental data focusing on lean 1,3-butadiene combustion at the presented conditions. In all cases presented in this work, the chemical kinetics mechanisms over predict the ignition delay time proven though experimentation.

CHAPTER FIVE: CONCLUSIONS

In conclusion, 1,3-butadiene is an important intermediate species during the combustion of real fuels like gasoline, diesel and jet fuel. In this work, the combustion of lean 1,3-butadiene mixtures were studied behind the reflected shock wave in a shock tube. Ignition delay times and 1,3-butadiene time-histories for three different mixtures are reported. Ignition delay times were determined by four different definitions: the point of maximum radical concentration, maximum rate of radical formation extrapolated to a baseline value of radicals, the point when 2/3 of the initial fuel concentration is depleted and by the maximum rate of pressure increase extrapolated to a baseline value of pressure. 1,3-Butadiene time-histories was determined by absorption spectroscopy using a CO_2 laser operating at the P14 line near 10.532 μm. To the best of the authors knowledge this work is the first to include 1,3-butadiene time-histories during 1,3-butadiene combustion in a shock tube measured with absorption spectroscopy. As well as, the first work to study 1,3-butadiene combustion using N_2 as a diluent in a shock tube.

Results obtained from this work were compared to two common chemical kinetics mechanisms, Aramco 2.0 mechanism and Lawrence Livermore National Laboratory (LLNL) Gasoline Surrogate mechanism using CHEMKIN PRO under constant pressure and internal energy conditions. In all cases, both mechanisms over predict the ignition delay time of lean 1,3-butadiene combustion. Future works should include refinement of chemical kinetics models to better match experimental results presented in this work by validating rate coefficients for major reactions during 1,3-butadiene combustion.

REFERENCES

1. Scott, R.B., et al., *Thermodynamic properties of 1, 3-butadiene in the solid, liquid, and vapor states.* J. Res. Natl. Bur. Std, 1945. **35**: p. 35-89.
2. Hansen, N., et al., *Benzene formation in premixed fuel-rich 1, 3-butadiene flames.* Proceedings of the Combustion Institute, 2009. **32**(1): p. 623-630.
3. DAGAUT*, P. and M. Cathonnet, *The oxidation of 1, 3-butadiene: Experimental results and kinetic modeling.* Combustion science and technology, 1998. **140**(1-6): p. 225-257.
4. Laskin, A., *Detailed kinetic modeling of 1, 3-butadiene oxidation at high temperatures.* International Journal of Chemical Kinetics, 2000. **32**(10): p. 589-614.
5. Aparna M. Koppikar, C.W., Teresa Leavens, Lawrence Valcovic, Carole Kimmel, Rosmarie Faust, Jennifer Jinot and Aparna M. Koppikar *Health Assessment of 1,3-Butadiene.* 2002, National Center for Environmental Assessment–Washington Office.
6. Yao, M., Z. Zheng, and H. Liu, *Progress and recent trends in homogeneous charge compression ignition (HCCI) engines.* Progress in Energy and Combustion Science, 2009. **35**(5): p. 398-437.
7. Yap, D., et al., *Natural gas HCCI engine operation with exhaust gas fuel reforming.* International Journal of Hydrogen Energy, 2006. **31**(5): p. 587-595.
8. Bowman, C.T., *A shock-tube investigation of the high-temperature oxidation of methanol.* Combustion and Flame, 1975. **25**: p. 343-354.
9. Gloersen, P., *Some Unexpected Results of Shock‐ Heating Xenon.* The Physics of Fluids, 1960. **3**(6): p. 857-870.
10. Allen, M.G., *Diode laser absorption sensors for gas-dynamic and combustion flows.* Measurement Science and Technology, 1998. **9**(4): p. 545.
11. Stark, G., J. Brault, and M. Abrams, *Fourier-transform spectra of the A 2 Σ+–X 2 Π Δv= 0 bands of OH and OD.* JOSA B, 1994. **11**(1): p. 3-32.
12. Davidson, D., et al., *Measurements of the OH AX (0, 0) 306 nm Absorption Bandhead at 60 atm and 1735 K.* Journal of Quantitative Spectroscopy and Radiative Transfer, 1996. **55**(6): p. 755-762.
13. Liu, J.T., et al., *Near-infrared diode laser absorption diagnostic for temperature and water vapor in a scramjet combustor.* Applied Optics, 2005. **44**(31): p. 6701-6711.
14. Koroglu, B., et al., *Shock tube ignition delay times and methane time-histories measurements during excess CO 2 diluted oxy-methane combustion.* Combustion and flame, 2016. **164**: p. 152-163.
15. Gauthier, B., D.F. Davidson, and R.K. Hanson, *Shock tube determination of ignition delay times in full-blend and surrogate fuel mixtures.* Combustion and Flame, 2004. **139**(4): p. 300-311.
16. Vasu, S.S., et al., *n-Dodecane oxidation at high-pressures: Measurements of ignition delay times and OH concentration time-histories.* Proceedings of the Combustion Institute, 2009. **32**(1): p. 173-180.
17. Healy, D., et al., *Isobutane ignition delay time measurements at high pressure and detailed chemical kinetic simulations.* Combustion and Flame, 2010. **157**(8): p. 1540-1551.
18. Burcat, A., K. Scheller, and A. Lifshitz, *Shock-tube investigation of comparative ignition delay times for C1-C5 alkanes.* Combustion and Flame, 1971. **16**(1): p. 29-33.

19. He, X., et al., *An experimental and modeling study of iso-octane ignition delay times under homogeneous charge compression ignition conditions.* Combustion and Flame, 2005. **142**(3): p. 266-275.
20. Cole, J., et al., *Formation mechanisms of aromatic compounds in aliphatic flames.* Combustion and Flame, 1984. **56**(1): p. 51-70.
21. Fournet, R., J. Bauge, and F. Battin- Leclerc, *Experimental and modeling of oxidation of acetylene, propyne, allene and 1, 3- butadiene.* International journal of chemical kinetics, 1999. **31**(5): p. 361-379.
22. Brezinsky, K., E. Burke, and I. Glassman. *The high temperature oxidation of butadiene.* in *Symposium (International) on Combustion.* 1985. Elsevier.
23. Stranic, I., D.F. Davidson, and R.K. Hanson, *Shock tube measurements of the rate constant for the reaction cyclohexene→ ethylene+ 1, 3-butadiene.* Chemical Physics Letters, 2013. **584**: p. 18-23.
24. Oehlschlaeger, M.A., D.F. Davidson, and R.K. Hanson, *High-temperature thermal decomposition of benzyl radicals.* The Journal of Physical Chemistry A, 2006. **110**(21): p. 6649-6653.
25. Hidaka, Y., et al., *Shock-tube study of CH2O pyrolysis and oxidation.* Combustion and flame, 1993. **92**(4): p. 365-376.
26. Mehl, M., et al., *Kinetic modeling of gasoline surrogate components and mixtures under engine conditions.* Proceedings of the Combustion Institute, 2011. **33**(1): p. 193-200.
27. Metcalfe, W.K., et al., *A hierarchical and comparative kinetic modeling study of C1− C2 hydrocarbon and oxygenated fuels.* International Journal of Chemical Kinetics, 2013. **45**(10): p. 638-675.